Fast Fluid Antenna Multiple Access Enabling Massive Connectivity

Kai-Kit Wong, *Fellow, IEEE,* Kin-Fai Tong, *Senior Member, IEEE,* Yu Chen, *Member, IEEE,* and Yangyang Zhang

***Abstract*—Massive connectivity over wireless channels relies on aggressive spectrum sharing techniques. Conventionally, this may be achieved by sophisticated signal processing and optimization of applying multiple antennas and/or complex multiuser decoding at each user terminal (UT). Different from previous methods, this letter proposes a radical approach for massive connectivity, which employs fluid antenna at each UT to exploit the interference null, created naturally by multipath propagation and the randomness of UT's data, on a symbol-by-symbol basis for multiple access. The proposed fast fluid antenna multiple access (f-FAMA) system adopts a large, distributed antenna array at the base station (BS) to transmit each UT's signal from each of the BS antennas and lets each UT overcome the interference on its own using its fluid antenna. Our main contribution is a technique that estimates the best port of fluid antenna for reception at every symbol instance. The proposed approach needs only cross-correlation calculations and single-user decoding at each UT and requires no precoding at the BS. Simulation results demonstrate that for a BS with 16 antennas supporting 16 co-channel users, a multiplexing gain of 14.87 is achieved even when the channel has a strong line-of-sight (LoS) and multipath is few. The multiplexing gain can also rise to 24.36 if a 30-antenna BS is serving 30 co-channel users.**

***Index Terms*—Capacity, Distributed antennas, Fluid antenna, Massive connectivity, MIMO, Multiple access.**

I. Introduction

MASSIVE machine type communications (mMTC) in the fifth-generation (5G) mobile networks aims to support high connection density in the order of 1 million connections per square kilometer. With a forecast of having 30 billion or more internet-of-things (IoT) devices by 2030, mMTC in the sixth-generation (6G) era will undoubtedly seek to meet more ambitious requirements [1]. Common understanding tends to rely on the use of multiple-input multiple-output (MIMO) at the base station (BS) for interference avoidance and grant-free non-orthogonal multiple access (NOMA) to solve the resource collision issue and enhance the spectral efficiency.

Unfortunately, multiuser MIMO (including massive MIMO in 5G) requires channel state information (CSI) to be known at the BS and the optimization also gets harder if more user terminals (UTs) are involved, not to mention the overheads that follow. On the other hand, despite the capability of resolving interference at the UT side, NOMA needs complex multiuser detection to be carried out at the UTs and its use is therefore often limited to two co-channel users only. There seems to be a long way to go for achieving massive connectivity.

The work is supported in part by EPSRC under grant EP/W026813/1.

K. K. Wong and K. F. Tong are with the Department of Electronic and Electrical Engineering, University College London, London WC1E 7JE, United Kingdom. Corresponding author: kai-kit.wong@ucl.ac.uk.

Y. Chen is with Beijing University of Posts and Telecommunications, China.

Y. Zhang is with Kuang-Chi Science Limited, Hong Kong SAR, China.

Ideally, the multiple access technology for massive connectivity should have its complexity increasing only slowly with the number of UTs and does not overload the UTs too much. One emerging technology that may be the key to this is *fluid antenna* [2]. Fluid antenna represents any radiating structure that can change, on-demand, their shape, size and/or position to reconfigure the polarization, operating frequency, radiation pattern, and other performance metrics. In practice, it can be based on fluidic, conductive or dielectric material [3]–[7], or reconfigurable electronic switches and pixels [8]–[12].

One revolutionary aspect of this is that we can contemplate to have a software-controlled, position-switchable antenna that can maximize the reception performance by choosing the best position (i.e., port selection) in a predefined space. Recently, this idea has been explored for single-user systems, e.g., [13]–[17] and multiuser systems [18]–[20]. Of particular relevance to this letter is the way in which fluid antenna deals with co-channel interference in the multiuser scenarios.

Specifically, a UT can use its fluid antenna to skim through a large collection of fading envelopes from the ports and then switches the radiating element to the one where the co-channel interference naturally disappears due to multipath fading and no preprocessing of the multiuser signals is required. In [18], it was hypothesized that the fluid antenna at a UT could track the null of sum-interference on a symbol-by-symbol basis while [20] considered an arguably more practical setup in which the fluid antenna settled on the port where the channel envelopes of all the interferers faded, and only needed to switch if the channels had changed. The approach, referred to as slow fluid antenna multiple access (s-FAMA), in [20] can support several users (≤ 5) on the same time-frequency channel.

Nonetheless, the real impact may come from the fast fluid antenna multiple access (f-FAMA) system in [18] that shows massive connectivity of tens or even hundred of UTs without precoding at the BS, all by a single fluid antenna at each UT. The acquisition of CSI at the BS is thus not needed. The main challenge, however, is that f-FAMA needs each UT to identify the best port (i.e., the port where the null of sum-interference occurs) on its own without coordination and switch to it for every symbol instance, which is not known achievable.[1]

Motivated by this, in this letter, we aim to address the port selection problem for f-FAMA when each UT only has access to the received signals at the ports of its fluid antenna and knows the fading envelopes of its own channel. There is no

[1]Note that the switching delay between ports can be negligible if reconfigurable pixel designs [8]–[12] are used for the fluid antenna. However, the same cannot be said if liquid-based fluid antenna technologies [3]–[7] are used and their delay will make it impossible for f-FAMA systems.

prior information about the channel and data statistics of the interferers. To address this, our approach attempts to estimate the sum-interference plus noise signals over all the ports given only the knowledge of its own channel, and we achieve this by recognizing the fact that the UT's own channel and the sum-interference should be dissimilar and uncorrelated, and study the use of a number of similarity and cross-correlation measures. This letter uses a general channel model that includes a direct line-of-sight (LoS) and an arbitrary number of non-LoS paths that can represent microwave and millimeter-wave (mmWave) channels by choosing appropriate parameters. In addition, a distributed antenna array at the BS is adopted so that each BS antenna sees different scatterers before the UTs to ensure sufficient channel rank to support a large number of UTs. Our results illustrate that f-FAMA can achieve massive connectivity without precoding nor multiuser detection and confirm the importance of using distributed BS antennas.

II. The f-FAMA Network

A. System and Channel Model

We consider a downlink system where the BS is equipped with N_t fixed antennas spread[2] over a wide area to communicate with U single-antenna UTs. Each BS antenna is in charge of transmitting one UT's signal to the intended UT.[3] Each UT has an N-port fluid antenna with a physical size of $W\lambda$ where λ is the wavelength. The parameter N represents the number of preset positions (i.e., ports) evenly distributed over the space of $W\lambda$ that the radiating element can be switched to, and hence can be interpreted as the antenna's resolution.

At the k-th port of UT u, the received signal, with the time index omitted, can be written as

$$r_k^{(u)} = g_k^{(u,u)} s_u + \sum_{\substack{\tilde{u}\neq u \\ u=1}}^{U} g_k^{(\tilde{u},u)} s_{\tilde{u}} + \eta_k^{(u)}, \tag{1}$$

where $g_k^{(\tilde{u},u)}$ denotes the complex channel from the $\tilde{u}$-th BS antenna to the k-th port of UT u with $\mathrm{E}[|g_k^{(\tilde{u},u)}|^2] = \Omega$, $\eta_k^{(u)}$ denotes the zero-mean complex Gaussian noise at the k-th port of UT u with variance of σ_η^2, and s_u represents the information symbol for UT u with $\mathrm{E}[|s_u|^2] = \sigma_s^2$. The received average signal-to-noise ratio (SNR) at each port is defined as $\Gamma \triangleq \frac{\Omega\sigma_s^2}{\sigma_\eta^2}$.

While it may be typical to assume rich scattering in modelling the channel $g_k^{(\tilde{u},u)}$, this assumption will be unsuitable if the mmWave band is considered. For this reason, we employ a more general finite-scatterer channel model that can model the scenarios in the mmWave band and also rich scattering as a special case [21]. The model consists of a specular component (i.e., LoS) and N_p scattered components (i.e., non-LoS). For the specular component, it has an azimuth angle-of-arrival (AoA), θ_0 (with the UT index omitted for conciseness), and an elevation AoA, ϕ_0, while the scattered components have the azimuth AoAs, $\{\theta_\ell\}_{\ell=1}^{N_p}$ and elevation AoAs, $\{\phi_\ell\}_{\ell=1}^{N_p}$. As a consequence, the channel, $g_k^{(\tilde{u},u)}$, can be expressed as

$$g_k^{(\tilde{u},u)} = \sqrt{\frac{K\Omega}{K+1}} e^{j\alpha^{(\tilde{u},u)}} e^{-j\frac{2\pi(k-1)W}{N-1}\sin\theta_0^{(\tilde{u},u)}\cos\phi_0^{(\tilde{u},u)}} + \sum_{\ell=1}^{N_p} a_\ell^{(\tilde{u},u)} e^{-j\frac{2\pi(k-1)W}{N-1}\sin\theta_\ell^{(\tilde{u},u)}\cos\phi_\ell^{(\tilde{u},u)}}, \tag{2}$$

where K denotes the Rice factor (i.e., the power ratio between the specular and scattered components), $\alpha^{(\tilde{u},u)}$ is the random phase of the specular component, and $a_\ell^{(\tilde{u},u)}$ is the random complex coefficient of the ℓ-th scattered path. By definition, we have $\mathrm{E}[\sum_\ell |a_\ell^{(\tilde{u},u)}|^2] = \frac{\Omega}{K+1}$. If $N_p \to \infty$, then the sum of the scattered components will be Gaussian distributed due to central limit theorem. The angle of departures (AoDs) from the BS antennas are not considered here because the BS antennas are located far apart from each other and each of them sees different scatterers. The performance of f-FAMA using co-located BS antennas will be examined in Section IV.

B. Port Selection

In the f-FAMA network, each UT is required to switch to its best port k^* for every symbol instance. That is,[4]

$$k^* = \arg\max_k \frac{\left|g_k^{(u,u)} s_u\right|^2}{\left|\sum_{\substack{\tilde{u}\neq u \\ u=1}}^{U} g_k^{(\tilde{u},u)} s_{\tilde{u}} + \eta_k^{(u)}\right|^2} \overset{(a)}{=} \arg\max_k \frac{\left|g_k^{(u,u)}\right|^2}{\left|\tilde{g}_k^{(u)}\right|^2}, \tag{3}$$

where in (a), s_u in the numerator disappears because this is a constant over all the ports. Apparently, the maximum occurs when the instantaneous sum-interference plus noise becomes the smallest. Evidently, this depends on how the superposition of the interferers' data, their channels and the noise becomes, which is different from the s-FAMA system that only exploits the fades of the interferers' channels. It is understood that the interference null for f-FAMA will be more likely to occur than for s-FAMA. As a result, an enhanced interference rejection capability for massive connectivity is anticipated.

C. Multiplexing Gain

The performance of each UT can be characterized by outage probability when a target signal-to-interference plus noise ratio (SINR), γ, is set. To align with the methodology of f-FAMA in (3), we define an outage event as the occurrence of the instantaneous SINR being less than γ for a symbol. In other

[2]The use of distributed BS antennas is to ensure that the network capacity is not limited by the number of scatterers in the mmWave case.

[3]Distributed BS antennas are normally assigned to serve users based on their distances so that less transmit power is needed to achieve a given reception performance at each user. With perfect power control and antenna selection, the model is as if the users suffer from no pathloss and all the users are statistically identical. For this reason, this letter assumes, without loss of generality, that the u-th BS antenna is serving the u-th UT.

[4]Conceptually, selecting a port in a fluid antenna system is indeed similar to a traditional antenna selection system. However, there are fundamental operational differences between them. First, selection combining using multiple fixed antennas tend to have antenna spacing of at least $\frac{\lambda}{2}$ for diversity while the ports of a fluid antenna in the f-FAMA system should be as close as possible to ensure sufficient spatial resolution to access the sum-interference plus noise null for multiple access. In particular, the selection of the channel in (3) is not purely based on the strongest magnitude of the channels but rather the maximization of the instantaneous energy of the desired channel and that of the sum-interference plus noise signal in the f-FAMA system.

words, the outage probability for UT u can be defined as

$$p_{\text{out}} \triangleq \text{Prob}\left(\max_k \frac{\left|g_k^{(u,u)} s_u\right|^2}{\left|\tilde{g}_k^{(u)}\right|^2} < \gamma\right). \tag{4}$$

Assuming that all the UTs have identical channel statistics and each UT has a fixed coding rate derived from the SINR target, the network multiplexing gain is given by [18]

$$m = U(1 - p_{\text{out}}). \tag{5}$$

III. Proposed Algorithms

To perform (3), however, the u-th UT is required to know, $\{\tilde{g}_k^{(u)}\}_{\forall k}$, i.e., the instantaneous sum-interference plus noise at all the ports, in order to compute the ratios for maximization. If this is available, the maximization will be straightforward. In this letter, we assume that UT u only knows its own channel $\{g_k^{(u,u)}\}_{\forall k}$ and has no prior knowledge about the channel and data statistics of the interferers and noise. Our objective is to develop a method to estimate $\{\tilde{g}_k^{(u)}\}_{\forall k}$ given the knowledge of $\{g_k^{(u,u)}\}_{\forall k}$ and the type of digital modulation it employs. In particular, we assume, without loss of generality, that s_u is drawn from quadrature phase shift keying (QPSK) symbols. Our method can be extended to other modulation schemes.

From (1), the estimate of $\{\tilde{g}_k^{(u)}\}_{\forall k}$ can be obtained by

$$\widehat{\tilde{g}_k^{(u)}} = r_k^{(u)} - g_k^{(u,u)} \tilde{s}_u, \tag{6}$$

for some $\tilde{s}_u \in \{\frac{1}{\sqrt{2}}(\pm 1 \pm j)\}$. In other words, there are only a finite number of choices for $\tilde{s}_u$ to decide on the best estimate. Now, the remaining task is to find a metric to figure out which $\tilde{s}_u$ returns the best estimate. Before we do this, we first realize that the complex channel envelopes $\{g_k^{(u,u)}\}_{\forall k}$ and the sum-interference-plus noise signals $\{\tilde{g}_k^{(u)}\}_{\forall k}$ should be independent or dissimilar by nature. For this reason, we consider several cross-correlation and similarity metrics as follows.

- **Pearson's cross-correlation**—this metric finds the cross-correlation between the channel sequence $\{g_k^{(u,u)}\}_{\forall k}$ and the estimated sequence $\{\widehat{\tilde{g}_k^{(u)}}\}_{\forall k}$ by

$$\mathcal{D}\left(\{g_k^{(u,u)}\}_{\forall k}, \{\widehat{\tilde{g}_k^{(u)}}\}_{\forall k}\right) = \frac{\left|\left(\boldsymbol{g}^{(u,u)} - \frac{1}{N}\sum_k g_k^{(u,u)}\right)^\dagger \left(\widehat{\tilde{\boldsymbol{g}}^{(u)}} - \frac{1}{N}\sum_k \widehat{\tilde{g}_k^{(u)}}\right)\right|}{\|\boldsymbol{g}^{(u,u)}\| \|\widehat{\tilde{\boldsymbol{g}}^{(u)}}\|} \tag{7}$$

  where

$$\begin{cases} \boldsymbol{g}^{(u,u)} \triangleq [g_1^{(u,u)} \; g_2^{(u,u)} \cdots g_N^{(u,u)}]^T, \\ \widehat{\tilde{\boldsymbol{g}}^{(u)}} \triangleq [\widehat{\tilde{g}_1^{(u)}} \; \widehat{\tilde{g}_2^{(u)}} \cdots \widehat{\tilde{g}_N^{(u)}}]^T, \end{cases} \tag{8}$$

  the superscript T and $\dagger$ denote the transpose and hermitian operation, respectively, $|\cdot|$ returns the modulus of a complex number, $\|\cdot\|$ outputs the 2-norm of a vector.
- **Cosine of angle**—This metric is similar to the Pearson's cross-correlation except that the means of the sequences are not removed when computing the cross-correlation. In particular, the result gives the cosine of the angle of the dot product of the two sequences. That is,

$$\mathcal{D}(\cdot,\cdot) = \frac{\left|\left(\boldsymbol{g}^{(u,u)}\right)^\dagger \left(\widehat{\tilde{\boldsymbol{g}}^{(u)}}\right)\right|}{\|\boldsymbol{g}^{(u,u)}\| \|\widehat{\tilde{\boldsymbol{g}}^{(u)}}\|}. \tag{9}$$

- **Mean similarity**—It is possible to compute the similarity between two sequences. Similarity between two numbers, x and y, is usually defined as $\frac{|x-y|}{|x|+|y|}$. The mean similarity therefore can be found by

$$\mathcal{D}(\cdot,\cdot) = \frac{1}{N}\sum_{k=1}^{N}\left[1 - \frac{\left|g_k^{(u,u)} - \widehat{\tilde{g}_k^{(u)}}\right|}{|g_k^{(u,u)}| + |\widehat{\tilde{g}_k^{(u)}}|}\right]. \tag{10}$$

- **Root-mean-square (RMS) similarity**—A similar similarity measure computes the RMS of similarity of the two sequences given by

$$\mathcal{D}(\cdot,\cdot) = \sqrt{\frac{1}{N}\sum_{k=1}^{N}\left[1 - \frac{\left|g_k^{(u,u)} - \widehat{\tilde{g}_k^{(u)}}\right|}{|g_k^{(u,u)}| + |\widehat{\tilde{g}_k^{(u)}}|}\right]^2}. \tag{11}$$

- **Peak similarity**—Another similarity measure defines the similarity of each pair relative to the peak of the pair of the two sequence, which is given by

$$\mathcal{D}(\cdot,\cdot) = \frac{1}{N}\sum_{k=1}^{N}\left[1 - \frac{\left|g_k^{(u,u)} - \widehat{\tilde{g}_k^{(u)}}\right|}{2\max\left\{|g_k^{(u,u)}|, |\widehat{\tilde{g}_k^{(u)}}|\right\}}\right]. \tag{12}$$

To summarize, the estimate of $\{\tilde{g}_k^{(u)}\}_{\forall k}$ can be found as

$$\widehat{\tilde{g}_k^{(u)}} = r_k^{(u)} - g_k^{(u,u)} s_u^*, \tag{13}$$

where

$$s_u^* = \arg \min_{s_u \in \left\{\frac{1}{\sqrt{2}}(\pm 1 \pm j)\right\}} \mathcal{D}\left(\{g_k^{(u,u)}\}_{\forall k}, \{\widehat{\tilde{g}_k^{(u)}}\}_{\forall k}\right) \tag{14}$$

where the distance measure, $\mathcal{D}(\cdot,\cdot)$, can be chosen from the cross-correlation or similarity measures described above. The proposed algorithm is given in **Algorithm 1**. After we have obtained the estimate, the best port for f-FAMA is found by

$$k^* = \arg\max_k \frac{\left|g_k^{(u,u)}\right|^2}{\left|\widehat{\tilde{g}_k^{(u)}}\right|^2}. \tag{15}$$

One point worth mentioning is that it is possible to know only a subset of the channels $\{g_k^{(u,u)}\}$ and exploit the spatial correlation over the ports using techniques such as machine learning to infer the best port. In this letter, nevertheless, we assume full knowledge of $\{g_k^{(u,u)}\}$ to simplify our discussion and will study this in future work. Note that such approach was explored for single-user fluid antenna systems in [22].

Algorithm 1: Estimation of $\{\tilde{g}_k^{(u)}\}_{\forall k}$

Given the digital symbols $s_u \in \{q_1, q_2, \ldots, q_M\}$
For $i = 1$ to M
  $\widehat{s_u} = q_i$
  $\widehat{\tilde{g}_k^{(u)}} = r_k^{(u)} - g_k^{(u,u)} s_u$
  Compute $d_i = \mathcal{D}\left(\{g_k^{(u,u)}\}_{\forall k}, \{\widehat{\tilde{g}_k^{(u)}}\}_{\forall k}\right)$
End for
$i^* = \arg\min_i d_i$
$\widehat{\tilde{g}_k^{(u)}} = r_k^{(u)} - g_k^{(u,u)} q_{i^*}$
Return $\widehat{\tilde{g}_k^{(u)}}$

IV. Simulation Results

In this section, we present simulation results to investigate the performance of the proposed algorithm with the different distance measures. We assume that QPSK is used for modulating the information at the BS to the UTs. The channel model used has already been described in (2) which considers a LoS path with Rice factor K and N_p non-LoS paths. In particular, with the mmWave band in mind, we choose $(K, N_p) = (7, 2)$. Unless specified otherwise, we set the average SNR at each port as $\Gamma = 35$dB and the SINR threshold as $\gamma = 10$dB.

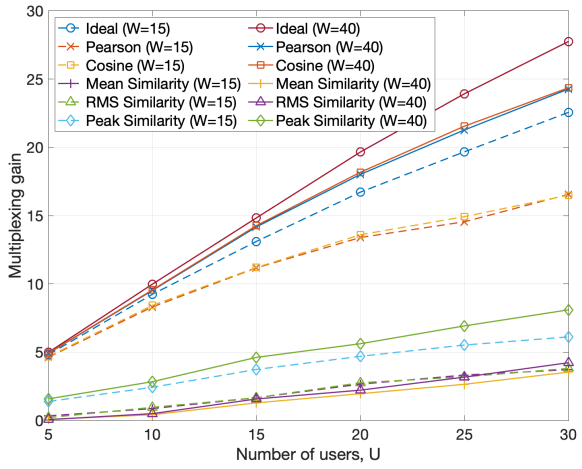

Fig. 1. Multiplexing gain for f-FAMA with different distance measures when $N = 1000$, $\Gamma = 35$dB, $\gamma = 10$dB and $(K, N_p) = (7, 2)$.

The simulation results in Fig. 1 are provided for the multiplexing gain of f-FAMA with different distance measures against the number of UTs, U, when the number of ports, N, at each UT's fluid antenna is 1000 and for sizes $W = 15$ and $W = 40$. Note that $W = 15$ may be interpreted as a size of 17cm at 26GHz while $W = 40$ may mean a size of 17cm at 70GHz. The results labelled as 'Ideal' correspond to the case when the ratios in (3) are perfectly known for port selection. As we can see, the multiplexing gain (i.e., capacity scaling) increases with the number of UTs, meaning that f-FAMA can resolve the interference effectively. Moreover, as expected, the multiplexing gain improves if W is larger. We also observe that cosine of angle and Pearson's cross-correlation impress while the similarity metrics perform relatively badly. In particular, if $U = 15$, then f-FAMA with cosine of angle can achieve a multiplexing gain of 11 for $W = 15$ and 14 for $W = 40$. This indicates over 10 times capacity gain over a single user system occupying the same bandwidth. A higher capacity gain can be seen for the $U = 30$ case where f-FAMA with cosine of angle delivers a multiplexing gain of 24 for $W = 40$.

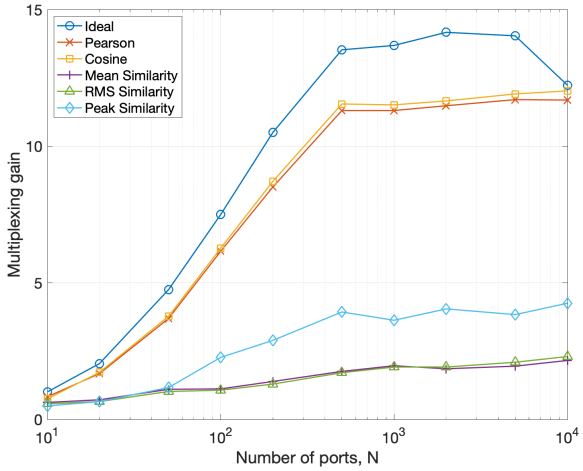

Fig. 2. Multiplexing gain for f-FAMA with different distance measures when $N_t = U = 16$, $W = 15$, $\Gamma = 35$dB, $\gamma = 10$dB and $(K, N_p) = (7, 2)$.

The results in Fig. 2 study how the performance of f-FAMA with different distance measures changes with the number of ports, N. The results are provided for the case with $U = 16$ UTs, each with $W = 15$. As expected, the multiplexing gain performance generally improves as N increases. Nonetheless, the capacity gain saturates if N is very large. This indicates that $N = 500$ is enough to achieve the maximum capacity gain in this case.[5] Further gain will need a larger W.

Fig. 3 considers the same settings as before to study how the capacity performance of the proposed f-FAMA algorithm changes if the average received SNR, Γ, changes. Intuitively, one would expect that as Γ increases, the proposed algorithm should perform better but this appears not to be the case. The results illustrate that the multiplexing gain drops slightly as Γ increases. To explain this, we realize that the noise power only indicates the average noise energy over the ports but does not necessarily mean a worse performance because f-FAMA attempts to choose the port with the weakest (instantaneous) sum-interference plus noise signal. A larger noise power gives noise a larger dynamic range to cancel the sum-interference signal at each port, which gives rise to a capacity gain.

Finally, we investigate how important it is to use distributed BS antennas, as opposed to co-located BS antennas using the results in Fig. 4. We provide the multiplexing gain results for both the distributed (dashed lines) and co-located (solid lines)

[5]Note that in [18], the multiplexing gain for f-FAMA was shown to increase and then converge to U if N continues to increase. This is different from what we observe from the simulation results reported in this letter where the multiplexing gain can saturate before it reaches U even if N increases without bound. The main reason is that the channel model used in [18] was based on the generalized complex Gaussian model which tended to have higher diversity than it should [15]. The model (2) adopted in this letter in contrast provides a more accurate channel seen at each fluid antenna.

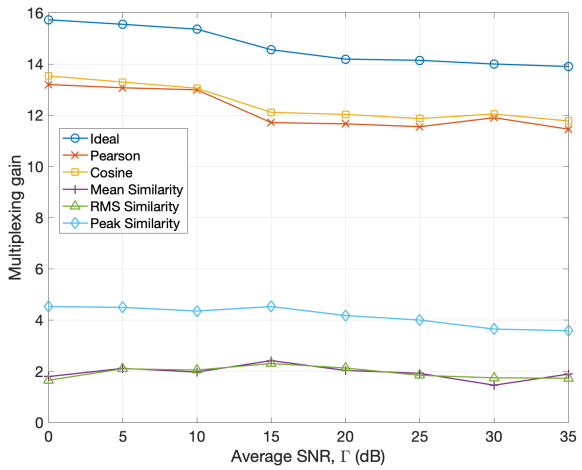

Fig. 3. Multiplexing gain for f-FAMA with different distance measures when $N_t = U = 16$, $W = 15$, $\gamma = 10$dB, $N = 1000$ and $(K, N_p) = (7, 2)$.

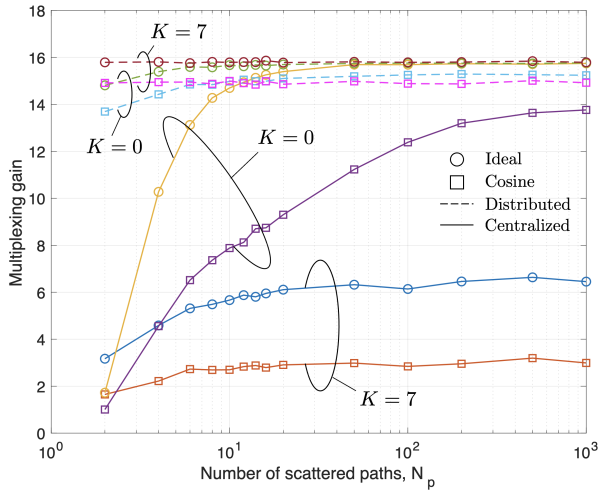

Fig. 4. Multiplexing gain comparison for f-FAMA with distributed and co-located BS antennas when $N_t = U = 16$, $W = 40$, $\Gamma = 35$dB, $\gamma = 10$dB, $N = 1000$ and for different channel conditions.

BS antenna cases, focusing only on the 'Ideal' and 'Cosine' approaches. For the co-located BS antenna case, the AoD from the BS antennas is brought back and all the BS antennas go through the same set of scatterers to reach the UTs [21]. From the results, we can observe that in the co-located BS antenna case, the multiplexing gain is greatly affected by the channel parameters, K and N_p, and is only good if there is no LoS, $K = 0$, and multipath is rich, i.e., large N_p. By contrast, the multiplexing gain remains large regardless of the values of K and N_p in the case of distributed BS antennas. This confirms the importance of the distributed setup for signal independence between the user signals for effective f-FAMA.

V. Conclusion

With the aim to unleash the performance of f-FAMA, this letter proposed an algorithm to estimate the instantaneous sum-interference plus noise signals for port selection. Our proposed algorithm was based on using different cross-correlation and similarity measures. The simulation results revealed that more than 10 times capacity gain could be achieved by using fluid antenna at each UT without the need of precoding at the BS nor multiuser detection at the UTs. The proposed approach does not require CSI at the BS and needs only the knowledge of the CSI of the desirable channel at the receiver's ports.

References

[1] N. H. Mahmood *et al.*, "White paper on critical and massive machine type communication towards 6G [White paper]," (6G Research Visions, No. 11). University of Oulu. [Online] http://urn.fi/urn:isbn:9789526226781.

[2] K. K. Wong, K. F. Tong, Y. Shen, Y. Chen, and Y. Zhang, "Bruce Lee-inspired fluid antenna system: Six research topics and the potentials for 6G," *Frontiers in Commun. and Netw., section Wireless Commun.*, 3:853416, Mar. 2022.

[3] A. M. Morishita, C. K. Y. Kitamura, A. T. Ohta, and W. A. Shiroma, "A liquid-metal monopole array with tunable frequency, gain, and beam steering," *IEEE Antennas Wireless Propag. Lett.*, vol. 12, pp. 1388–1391, 2013.

[4] A. Dey, R. Guldiken, and G. Mumcu, "Microfluidically reconfigured wideband frequency-tunable liquid-metal monopole antenna," *IEEE Trans. Antennas Propag.*, vol. 64, no. 6, pp. 2572–2576, Jun. 2016.

[5] C. Borda-Fortuny, K.-F. Tong, A. Al-Armaghany, and K. K. Wong, "A low-cost fluid switch for frequency-reconfigurable Vivaldi antenna," *IEEE Antennas Wireless Propag. Lett.*, vol. 16, pp. 3151–3154, 2017.

[6] A. Singh, I. Goode, and C. E. Saavedra, "A multistate frequency reconfigurable monopole antenna using fluidic channels," *IEEE Antennas Wireless Propag. Lett.*, vol. 18, no. 5, pp. 856–860, May 2019.

[7] Y. Huang, L. Xing, C. Song, S. Wang and F. Elhouni, "Liquid antennas: Past, present and future," *IEEE Open J. Antennas and Propag.*, vol. 2, pp. 473–487, 2021.

[8] B. A. Cetiner *et al.*, "Multifunctional reconfigurable MEMS integrated antennas for adaptive MIMO systems," *IEEE Commun. Mag.*, vol. 42, no. 12, pp. 62–70, Dec. 2004.

[9] A. Grau Besoli and F. De Flaviis, "A multifunctional reconfigurable pixeled antenna using MEMS technology on printed circuit board," *IEEE Trans. Antennas and Propag.*, vol. 59, no. 12, pp. 4413–4424, Dec. 2011.

[10] C. Chiu, J. Li, S. Song and R. D. Murch, "Frequency-reconfigurable pixel slot antenna," *IEEE Trans. Antennas and Propag.*, vol. 60, no. 10, pp. 4921–4924, Oct. 2012.

[11] D. Rodrigo, B. A. Cetiner and L. Jofre, "Frequency, radiation pattern and polarization reconfigurable antenna using a parasitic pixel layer," *IEEE Trans. Antennas and Propag.*, vol. 62, no. 6, pp. 3422–3427, Jun. 2014.

[12] S. Song and R. D. Murch, "An efficient approach for optimizing frequency reconfigurable pixel antennas using genetic algorithms," *IEEE Trans. Antennas and Propag.*, vol. 62, no. 2, pp. 609–620, Feb. 2014.

[13] K. K. Wong, A. Shojaeifard, K.-F. Tong and Y. Zhang, "Fluid antenna systems," *IEEE Trans. Wireless Commun.*, vol. 20, no. 3, pp. 1950–1962, Mar. 2021.

[14] L. Tlebaldiyeva, G. Nauryzbayev, S. Arzykulov, A. Eltawil and T. Tsiftsis, "Enhancing QoS through fluid antenna systems over correlated Nakagami-m fading channels," in *Proc. IEEE Wireless Commun. Netw. Conf. (WCNC)*, pp. 78–83, 10-13 Apr. 2022, Austin, TX, USA.

[15] M. Khammassi, A. Kammoun, and M.-S. Alouini, "A new analytical approximation of the fluid antenna system channel," [Online] arXiv preprint arXiv:2203.09318, 2022.

[16] C. Psomas, G. M. Kraidy, K. K. Wong, and I. Krikidis, "On the diversity and coded modulation design of fluid antenna systems," [Online] arXiv preprint arXiv:2205.01962, 2022.

[17] P. Mukherjee, C. Psomas, and I. Krikidis, "On the level crossing rate of fluid antenna systems," [Online] arXiv preprint arXiv:2205.01711, 2022.

[18] K. K. Wong, and K. F. Tong, "Fluid antenna multiple access," *IEEE Trans. Wireless Commun.*, vol. 21, no. 7, pp. 4801–4815, Jul. 2022.

[19] K. K. Wong, K. F., Tong, Y. Chen, and Y. Zhang, "Closed-form expressions for spatial correlation parameters for performance analysis of fluid antenna systems," *Elect. Letters*, vol. 58, no. 11, pp. 454–457, 2022.

[20] K. K. Wong, D. Morales-Jimenez, and K. F. Tong, "Slow fluid antenna multiple access," submitted to *IEEE Trans. Commun.*, 2022.

[21] O. E. Ayach, S. Rajagopal, S. Abu-Surra, Z. Pi and R. W. Heath, "Spatially sparse precoding in millimeter wave MIMO systems," *IEEE Trans. Wireless Commun.*, vol. 13, no. 3, pp. 1499–1513, Mar. 2014.

[22] Z. Chai, K. K. Wong, K. F. Tong, Y. Chen and Y. Zhang, "Port selection for fluid antenna systems," *IEEE Commun. Letters*, vol. 26, no. 5, pp. 1180–1184, May 2022.